Forming chemisorbed single-molecule junctions through loss of stable carbocations

Jazmine Prana,[a] Luana Zagami,[a] Kelly Yan,[a] Daniel Hernangómez-Pérez,*[,b] María Camarasa-Gómez,*[,c] and Michael S. Inkpen*[,a]

[a] *Department of Chemistry, University of Southern California, Los Angeles, CA 90089, USA*
[b] *CIC nanoGUNE BRTA, Tolosa Hiribidea, 76, 20018 Donostia-San Sebastián, Spain*
[c] *Centro de Física de Materiales (CFM-MPC) CSIC-UPV/EHU, 20018 Donostia-San Sebastián, Spain*

E-mail: d.hernangomez@nanogune.eu, maria.camarasa@ehu.eus, inkpen@usc.edu

ABSTRACT

Recent studies have found that "chemically inert" gold surfaces may drive S-C(sp^3) bond cleavage reactions in thioether (-SR) linker groups, providing access to single-molecule junctions with chemisorbed Au-S contacts following the elimination of R^+. Here we demonstrate that such transformations occur more readily at elevated temperatures, and perhaps surprisingly, in *non-polar* solvents. We further show that a greater proportion of chemisorbed bonds are formed when R = -CPh_3 or -C_7H_7 than when R = -^{t}Bu, consistent with the relative stability of $[^t\text{Bu}]^+ < [CPh_3]^+ \sim [C_7H_7]^+$ carbocations. Our contact chemistry assignments are supported by first principles transmission calculations, and we apply potential energy calculations to expose the relatively small influence of applied external electric fields on this bond breaking process. Together, this work provides a deeper understanding of reactivity at metal surfaces, of broad relevance to heterogenous catalysis and critical to the stability and function of molecular junctions and monolayers.

KEYWORDS – molecular electronics, interfacial reactions, carbocation chemistry, Lewis acids, single-molecule conductance, scanning tunneling microscope-based break junction method, DFT-NEGF, tritylium, tropylium

Interfacial bond-breaking and -forming processes form the fundamental basis of all heterogeneous catalytic processes used across chemical industry.[1,2] They also play an important role in anchoring molecular species to metal surfaces through chemisorption, enabling, for example, fundamental studies of electron transfer,[3] self-assembly,[4] or chemical reactivity,[5] as well as applications in biosensing[6] or catalysis.[7] A prototypical example in this context is the reaction of molecules comprising thiol (-SH) groups at the surface of gold to form adsorbed thiolates (-S-Au).[8] Here, the resulting chemisorbed bonds are distinguished from structurally related physisorbed -S(R)-Au interactions, formed with molecules comprising thioether groups (-SR), where the adsorbing species do not undergo any significant chemical change. Such differences in surface bonding interactions can be readily evaluated using metal/single molecule/metal junctions, devices which approach the limit of miniaturization for circuit elements used in computation or data storage. Here, chemisorbed sulfur, carbon, nitrogen, and oxygen contacts to gold and/or silver electrodes, formed from reactive groups such as thiols,[9,10] trialkylstannanes,[11] alkynes,[12,13] amines,[14] carboxylic acids,[15] and halides,[16,17] have been widely exploited to form single-molecule junctions with distinct transport properties. These contact chemistries have also been used to study the influence of applied external electric fields (EEFs), solvent environment, or electrochemical potential,[16,18] as well as temperature[19] on the competency and rate of chemical transformations occurring at electrode surfaces, using single-molecule conductance measurements to monitor reaction progress.

Recent reports have highlighted the possibility of forming junctions with chemisorbed Au-S bonds from components comprising thio-*tert*-butyl (-S^{t}Bu)[20,21] or 2,3-dihydrobenzo[b]thiophene[22] linker groups. For 4,4'-bis(tert-butylthio)-1,1'-biphenyl (**^{t}Bu**, **Figure 1**), it was proposed that coordination of the sulfur lone pair of -S^{t}Bu (a Lewis base) to an undercoordinated gold atom (serving as a Lewis acid) activates the S-C(sp^3) bond towards heterolytic cleavage.[20] In this scheme, -S-Au is formed from -S(^{t}Bu)-Au with the concurrent loss of [^{t}Bu]$^+$, a moderately stable tertiary carbocation;[23] drawing analogies to established solution-based reactions in which -^{t}Bu groups can be cleaved from -S^{t}Bu in the presence of Lewis acids such as $TiCl_4$/BBr_3.[24,25] Importantly, analogous S-C(sp^3) bond breaking processes were not observed in studies of related components comprising -SR linkers where R = methyl, ethyl, phenyl, *iso*-propyl, or *n*-dodecyl – groups that would form less stable primary/secondary carbocations through such reactions.[20] This work raises several additional questions, most notably: (1) what are the key factors influencing such surface-mediated bond breaking processes; (2) can additional evidence be presented in support of the proposed (carbocation

loss) mechanism; and (3) does this reactivity impact the interpretation of any previous investigations in molecular electronics involving thioether-substituted compounds?

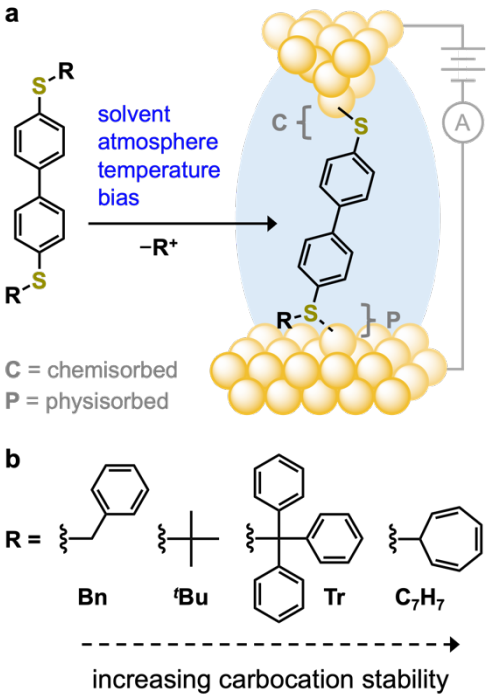

Figure 1. *In situ* S-C(sp^3) bond breaking reactions at the surface of gold electrodes are studied using molecular conductance measurements. **(a)** Single-molecule junctions (right) are formed from solution using molecular analytes (left) comprising a 4,4'-biphenyl backbone functionalized with different thioether linkers (-SR). While these linkers are typically used to form physisorbed (P) contacts to gold electrodes, they may also yield chemisorbed (C) contacts when R^+ is an appropriate leaving group. **(b)** Molecular structures of the linkers studied here, which are expected to generate carbocations of different stabilities following heterolytic S-C(sp^3) bond cleavage. Complete molecular structures of all analytes and solvents are provided in **Figure S1**. Using **^{t}Bu** (where R = -^{t}Bu), we probe the influence of solvent, atmosphere, temperature, and junction voltage bias (V_{bias}) on this interfacial bond-breaking process. By changing the R substituent it is possible to form junctions that exclusively comprise either P or C linkages.

Accordingly, here we present an expansive study that evaluates the impact of different reaction conditions and thioether substituents on the formation of chemisorbed contacts in model single-molecule junctions. Using **^{t}Bu**, we find that *in situ* S-C(sp^3) cleavage is favored at elevated temperatures, and perhaps surprising, in *non-polar* solvents, whereas the ambient environment (air or anhydrous nitrogen) and junction voltage bias (V_{bias}) appear to play a secondary role. Potential energy calculations of the S-C(sp^3) bond breaking process further reveal that EEFs only weakly perturb the barrier height. We further study analogous junction

components comprising -SR linkers designed to form carbocations of much greater stability than $[^{t}Bu]^{+}$ after heterolytic S-C(sp^3) bond cleavage: R = triphenylmethyl (**Tr**; forming the tritylium cation, $[CPh_3]^{+}$) or cycloheptatrienyl (**C_7H_7**; forming the tropylium cation, $[C_7H_7]^{+}$; **Figure 1b**). In strong support of the hypothesized reaction mechanism, and in contrast to measurements using **^{t}Bu**, both compounds *exclusively* form chemisorbed junctions. Finally, we show that a component with R = benzyl (**Bn**) forms only physisorbed junctions, indicating that benzyl cations ($[PhCH_2]^{+}$) are not eliminated under the measurement conditions tested. First principles transmission calculations confirm that physisorbed (intact) **^{t}Bu**, **Tr**, **C_7H_7**, and **Bn** junctions should exhibit a lower conductance than for analogous junctions with chemisorbed contacts; supporting the assignment of high conductance **^{t}Bu**, **Tr**, and **C_7H_7** features found experimentally to junctions with chemisorbed contacts.

We perform conductance measurements using the scanning tunneling microscope-based break junction (STM-BJ) method[9,26] with custom-built instrumentation described previously (see the **SI**).[19,27,28] Briefly, we apply a V_{bias} between a gold STM tip and substrate and measure the current (I) as the tip is pushed in and out of electrical contact. We plot the conductance ($G = I/V_{bias}$) as a function of tip–substrate displacement, obtaining traces that comprise step features around integer multiples of the conductance quantum ($G_0 = 2e^2/h = 7.748\times10^{-5}$ S). These features are attributed to the formation and breaking of atomic-sized gold contacts. After introducing 4,4'-biphenyl-based analytes as 0.1-1 mM solutions in various solvents, we observe new step features in these traces below 1 G_0 that correspond to the formation of single-molecule junctions (**Figure 1a**). We compile thousands of consecutively measured traces into one-dimensional (1D) conductance and two-dimensional (2D) conductance-displacement histograms (constructed without data selection), whereby the individual steps combine to form conductance features that are further analyzed to determine the most probable characteristics of the molecular junction. Synthetic methods for all noncommercially available 4,4'-biphenyl compounds are described in the **SI**.

We first present, in **Figure 2**, overlaid 1D histograms for measurements of **^{t}Bu** in different environments at $V_{bias} = \pm0.10$ V. Each histogram exhibits between 1-3 prominent conductance features, which we assign to junctions comprising two physisorbed contacts (PP, low conductance), one physisorbed and one chemisorbed contact (PC, medium conductance), or two chemisorbed contacts (CC, high conductance; **Figure 2a**). These peak assignments follow those made for previous studies of **^{t}Bu** in 1,2,4-trichlorobenzene (TCB), after accounting for small changes in conductance attributed to solvent effects.[29] While we observe significant experimental variation in the relative intensities of each peak (**Figures S3, S4**), the

data presented here exposes key trends in interfacial reactivity after appropriate analysis. Specifically, we deconvolute each histogram into three Gaussian peaks then use the peak areas to calculate the ratio of physisorbed to chemisorbed contacts (P/C; **Tables S1-3**). This quantitative metric facilitates straightforward comparisons of different measurements, where P/C > 1 indicates majority physisorbed contacts and P/C < 1 signifies majority chemisorbed contacts. The experimental variation in measurements of **^{t}Bu** has been tentatively attributed to differences in surface roughness near the junction that influence the local concentration of chemisorbed species generated at undercoordinated Lewis acidic atoms.[20] Here, for example, where lateral tip-substrate drift is low, repeated tip-substrate contact will significantly increase the surface roughness around the junction.[30]

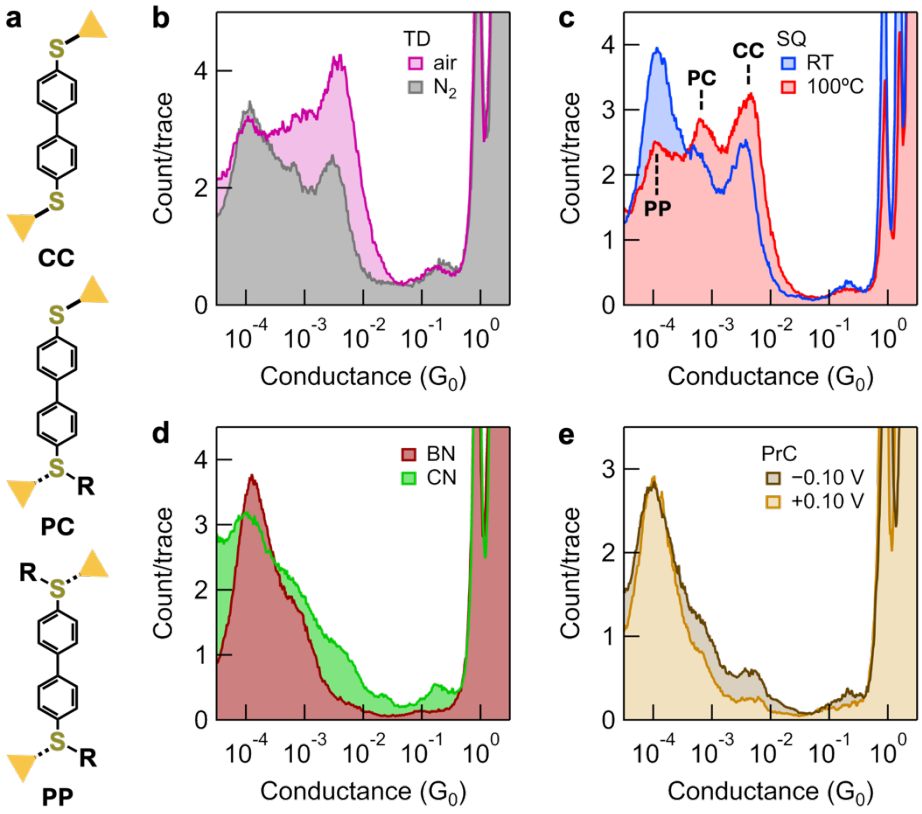

Figure 2. (a) Schematic illustration of CC, PC, and PP junction geometries (for **^{t}Bu**, R = −^{t}Bu). **(b-e)** Overlaid 1D conductance histograms obtained for measurements of **^{t}Bu** performed under different conditions (5,000 traces, V_{bias} = 0.10 V unless stated). Data from repeated measurements are provided in **Figures S3** and **S4**, and representative 2D conductance-displacement histograms are shown in **Figure S2**. **(a,b)** Measurements in non-polar solvents such as tetradecane (TD), or squalane (SQ; dipole moment, δ ~ 0 D, dielectric constant, ε ~ 2[31]), in air or under an inert nitrogen atmosphere, exhibit conductance peaks associated with PP, PC, and CC junction geometries. The relative intensity of each peak varies with experiment. After heating the system to 100°C in SQ, we consistently observe an increased relative intensity of PC and CC features compared to those in histograms from measurements at room temperature performed immediately before. **(c,d)** In contrast, measurements in polar solvents such as 1-bromonaphthalene (BN; δ = 1.55 D, ε = 4.77), 1-chloronaphthalene (CN; δ = 1.57 D, ε = 5.04), or propylene carbonate (PrC; δ = 4.9 D, ε = 66.14; V_{bias} = ±0.10 V) yield histograms that predominantly comprise PP features.[32]

In **Figures 2b-e** we contrast data from measurements in the non-polar solvents tetradecane (TD) and squalane (SQ; *top* panels), against those in polar solvents 1-bromonaphthalene (BN), 1-chloronaphthalene (CN), and propylene carbonate (PrC; *bottom* panels). This comparison clearly shows we obtain a lower P/C in non-polar solvents (P/C = 0.40-1.51) than in polar solvents (P/C = 1.50-4.47). The apparent decreased interfacial reactivity of **^{t}Bu** in solvents of higher polarity is perhaps surprising, given the well-established

trends for reactions involving carbocation intermediates in bulk solution.[33] In the bulk, polar solvents help to stabilize charged intermediates, decreasing the activation barrier and so increasing the reaction rate. Additional data analysis shows we cannot identify clear differences between P/C obtained from TD (or SQ) measurements in air or under an inert atmosphere at room temperature (**Tables S2**, **S3**). However, we do consistently observe a smaller P/C for SQ measurements at 100°C (0.46-0.61) relative to those performed at RT (1.16-1.21). This difference can be attributed to the more frequent higher energy molecular collisions that occur at elevated temperatures which can overcome the activation barrier for the interfacial reaction.

In rationalizing these observations, we note some key features of these surface-mediated solution-based reactions that distinguish them from bulk solution processes. *First*, where bond-breaking/forming steps occur at specific surface sites, the activity and accessibility of these sites should not be negatively impacted by other components of the system. TD and SQ are hydrophobic species which, unlike PrC, poorly solubilize adventitious water. We hypothesize that any dissolved water may serve as a competing Lewis base for the Lewis acidic undercoordinated gold adatoms,[28,34,35] or activated surface-adsorbed water ([($HO^{\delta-}$-$Au^{\delta+}$]$H^{\delta+}$) sites,[36] thought to mediate S-C(sp^3) bond breaking. Evaporative loss of adventitious water may also contribute to the enhanced reactivity observed in measurements in SQ at 100°C. Furthermore, in contrast to PrC, CN, or BN, TD and SQ do not themselves comprise any coordinating atoms (O, Cl, Br) that can interact with these sites.[29] The modulation of reaction rates, and even selectivity, through solvent interactions or adsorbates on heterogeneous catalyst surfaces is well-documented.[37,38] *Second*, a conducting metal substrate can itself serve to effectively solvate and stabilize proximal charged species (or dipoles) through polarization of the delocalized electrons in the bulk.[39,40] Stated differently, a metal surface may serve to lower activation barriers associated with the formation of charged intermediates even when reactions are performed in air, vacuum, or a low dielectric solvent.

We next evaluate the influence of the EEF on this *in situ* S-C(sp^3) bond breaking process, focusing on measurements in TD as these support a moderate baseline reactivity and because the low dielectric of this medium will minimize screening of the EEF.[41,42] In **Figure 3a**, we plot histograms obtained from sequential measurements of **^{t}Bu** at V_{bias} = 0.10 V, 0.75 V, and 0.10 V in air. As evidenced from this data, and repeated measurements in **Figure S3**, we cannot clearly discern the influence of EEF strength on P/C under these conditions due to experimental variability. Remarkably, however, when performing the experiments under an inert atmosphere inside of a glovebox we reproducibly observe a smaller P/C at V_{bias} = 0.75 V (0.40-0.84) compared to at V_{bias} = 0.1 V (0.93-1.17; **Figures 3b** and **S3**). We suggest that the

anhydrous, oxygen-free glovebox atmosphere helps to further minimize screening of the EEF and competition for available Lewis acidic surface sites. In addition, we reason the interfacial field may also further polarize and enhance the activity of reactive surface sites under these conditions.

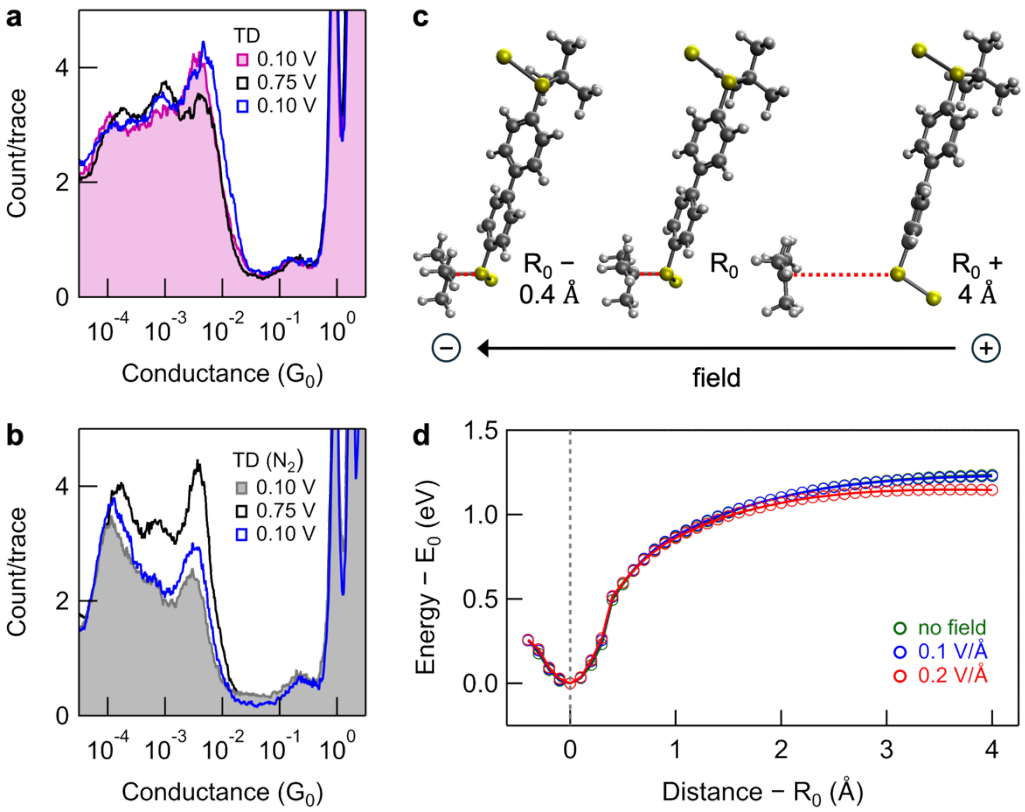

Figure 3. (a,b) Overlaid 1D histograms obtained from studies of **^{t}Bu** in TD measured sequentially at V_{bias} = 0.10 V, 0.75 V, and 0.10 V (each 5,000 traces). For studies in air, experimental variation obscures any possible influence of V_{bias} on the relative intensity of each peak feature (see **Figure S3a-c** for repeated measurements). For studies under nitrogen, we observe that the relative intensity of features associated with PC and CC junction geometries appears to increase with a higher V_{bias} (see **Figure S3d-e** for a repeated measurement). 2D histograms corresponding to these measurements are provided in **Figure S5**. **(c)** Optimized molecular geometries for **^{t}Bu**-Au_1 (applied field = 0 V/Å), obtained after constraining the distance between one S-C(sp^3) bond (dotted red lines) to different values relative to R_0 (the equilibrium bond length). The *tert*-butyl group is observed to planarize upon dissociation, as expected for the carbocation.[43] **(d)** Overlaid plots of distance against total energy for **^{t}Bu**-Au_1, normalized to R_0 and the equilibrium energy (E_0), respectively. For each plot, a different electric field is applied along the S-C(sp^3) bond, as indicated by the arrow in panel (c). For this reaction model, the field appears to exert only a small influence on the height of the energy barrier to bond dissociation.

To clarify the effect of the EEF on this interfacial reaction, we turn to density functional theory (DFT) calculations using **^{t}Bu**-Au_1 a model comprising **^{t}Bu** with a single gold atom connected to each sulfur group (**Figure 3c,d**). Following a recently reported method,[44] we calculate the total energy of **^{t}Bu**-Au_1 after geometry optimization while constraining the distance between the S-C(sp^3) atoms in one -S^{t}Bu group (see the **SI** for additional details). By compressing and stretching this bond, we obtain a bond dissociation curve (green line, **Figure 3d**) that resembles a Lennard-Jones potential, and normalize this to the equilibrium bond length, R_0 (dashed line) and energy, E_0. Notably, the *tert*-butyl group adopts a planar geometry upon dissociation, as expected for the carbocation (**Figure 3c**, right).[43] We subsequently repeat these calculations with an EEF of 0.1 V/Å and 0.2 V/Å along the constrained S–C axis (blue and red lines, respectively; **Figure 3d**). We find the EEF exerts only a small influence on the height of the energy barrier to bond dissociation, which decreases by ~7 meV from 0 to 0.1 V/Å, and by 82 meV from 0.1 to 0.2 V/Å. While the barrier calculated here is large, we reason that this will be smaller in experiments due to the presence of solvent and the proximal polarizable electrode. Furthermore, the conductance signal of products formed is likely amplified by their chemisorption on the surface even for slow reactions (they cannot easily diffuse away into the bulk). For completeness, we note that our bond dissociation curves do not comprise the transition state features that may be expected for such S_N1-like reaction coordinates. The observation of these features in related calculations, for example, that follow the formation of ^{t}BuOH from ^{t}BuCl, requires the inclusion of explicit solvent molecules.[45]

We subsequently targeted additional experiments using the new **Tr** and **C_7H_7** junction components (**Figure 1b**) to help corroborate the carbocation-loss mechanism for forming chemisorbed -S-Au contacts from **^{t}Bu**. These components comprise thioether groups capable of forming $[CPh_3]^+$ and $[C_7H_7]^+$ (with (4n + 2) aromatic character), carbocations that are *more stable* than $[^tBu]^+$ due to their extended, π-conjugated structures which stabilize the positive charge through resonance.[23,46] We reasoned that if the rate of S-C(sp^3) bond cleavage is strongly influenced by carbocation stability, **Tr** and **C_7H_7** should form junctions with a greater proportion of chemisorbed contacts than **^{t}Bu**. In **Figure 4a**, we plot overlaid 1D histograms from measurements of **Tr** and **C_7H_7** in TCB at V_{bias} = 0.10 V. Each exhibits a single conductance peak at 5.3×10^{-3} G_0 and 1.1×10^{-2} G_0, respectively. These values are greater than or equal to the conductance of junctions formed from **H** (~5×10^{-2} G_0), a species known to form chemisorbed junctions in solution,[10] and higher than the most conducting 4,4'-biphenyl junctions with physisorbed -S(R)-Au contacts (≤2.5×10^{-3} G_0).[20] This result indicates that both **Tr** and **C_7H_7** exclusively form junctions with chemisorbed contacts, in strong support of the

proposed *in situ* reaction mechanism (**Figure S7**). Interestingly, junctions formed from **C_7H_7** reproducibly exhibit a more intense peak feature with a conductance ~2× higher than those formed from **H** (**Figure S8**); an unexpected result that requires additional study.

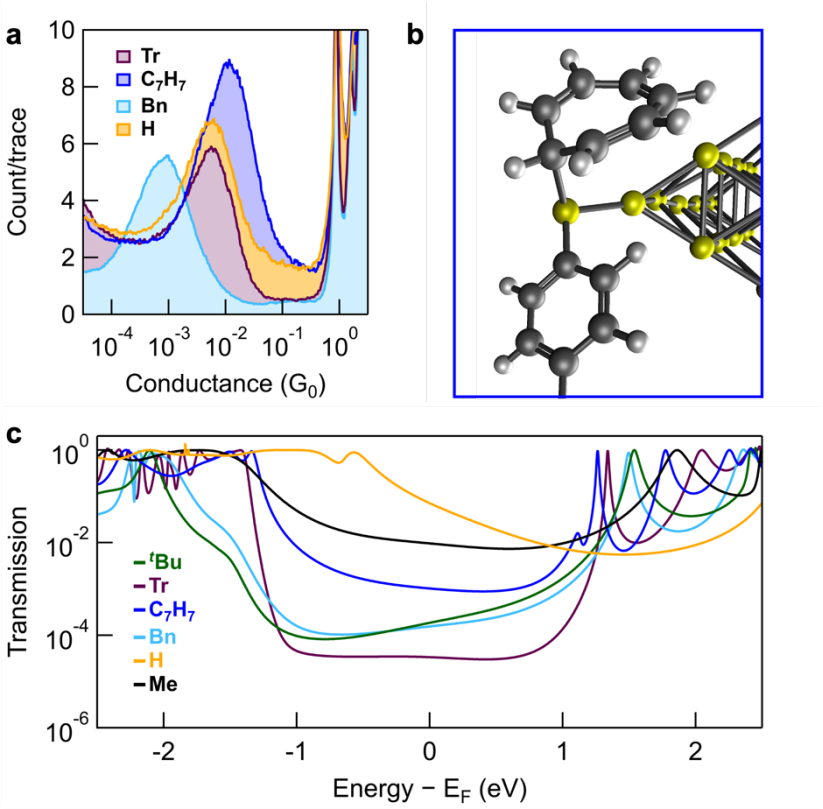

Figure 4. (a) Overlaid 1D histograms obtained from measurements of **Tr**, **C_7H_7**, **Bn**, and **H** in 1,2,4-trichlorobenzene (TCB; 10,000 traces, V_{bias} = 0.1 V). Histograms for **Tr** and **C_7H_7** exhibit single conductance peaks at or just above the conductance of **H**, a compound that is expected to form Au-S chemisorbed contacts. In contrast, histograms for **Bn** show a single feature at >5× lower conductance than **H** junctions. The 2D histograms corresponding to these measurements are provided in **Figures S6**. **(b)** Optimized geometry for **C_7H_7** junctions, showing a close-up view of the physisorbed contact. Additional geometries for all modelled junctions are shown in **Figure S10**. **(c)** Overlaid DFT-NEGF transmission calculations. In contrast to our experimental findings for **Tr** and **C_7H_7**, all intact thioethers with physisorbed -S(R)-Au contacts exhibit a lower calculated conductance relative to **H** modelled with chemisorbed -S-Au bonds. Together, this data supports the hypothesis that **Tr** and **C_7H_7** exclusively form junctions with CC geometries (following S-C(sp^3) cleavage and loss of tritylium/tropylium cations), whereas **Bn** exclusively forms junctions with PP geometries (no S-C(sp^3) cleavage occurs). We note that the low calculated conductance for physisorbed **^{t}Bu** junctions is in good agreement with the low experimental conductance peak features assigned to PP geometries (e.g., **Figure 2d,e**), and the results of earlier work.[20]

Finally, we explored the potential for **Bn** to undergo similar S-C(sp^3) bond breaking reactions at a gold surface. While the direct formation of primary benzyl cations ($[PhCH_2]^+$) would appear energetically unfavorable, the possibility that these species may undergo rearrangements to more stable $[C_7H_7]^+$ cations has long been debated.[47,48] Crucially, **Bn** comprises the same aryl-CH_2SR (R = H, Me) motif used elsewhere in molecular electronics, with assumed stability, to electronically decouple electrode and molecular backbone states,[49–52] or probe constructive quantum interference.[53] As shown in **Figures 4a** and **S9**, measurements of **Bn** in TCB or TD exhibit a single peak at a conductance significantly *lower* than the chemisorbed and physisorbed junctions formed from **H** and 4,4'-bis(methylthio)-1,1'-biphenyl (**Me**), respectively. Following previous reports, we attribute the lower conductance of **Bn** junctions to the relatively bulky benzyl substituent, which enforces junction geometries that serve to electronically decouple the electrode and molecular backbone states (discussed further below).[20,54,55] This in turn implies that **Bn** forms only physisorbed junctions, and that this S-C(sp^3) bond is indeed stable under these experimental conditions.

To further evaluate our experimental observations we turn to *ab initio* quantum transport calculations conducted within the framework of DFT and the non-equilibrium Green's function (NEGF) formalism, utilizing FHI-aims[56] in conjunction with the AITRANSS transport module (see the **SI** for additional details).[57–59] In **Figure 4c**, we display overlaid transmission calculations for **^{t}Bu**, **Tr**, **C_7H_7**, **Bn**, **H**, and **Me** model junctions. A representative optimized geometry for **C_7H_7** is shown in **Figure 4b**, giving a clear view of the physisorbed contact, with additional junction geometries provided in **Figure S10**. We focus here on the *trends* in calculated conductance rather than their absolute values, which are overestimated by >1 order of magnitude due to the well-known inherent limitations of generalized-gradient approximations applied in this context.[60,61]

We first observe that **H**, despite having the largest gas phase HOMO-LUMO gap (**Table S5**), exhibits the highest conductance. Here, transport is strongly dominated by the HOMO, which is broadened due to chemisorption and increased coupling with the electrode (CC geometry). Notably, all other physisorbed junctions (PP geometries) exhibit a lower conductance, with the Fermi level (E_F) positioned approximately at the midpoint of each HOMO-LUMO gap. The trends in calculated conductance for **H** (CC) > **Me** (PP) > **Bn** (PP) ~ **^{t}Bu** (PP) agree well with those assigned experimentally (**Figures 2**, **4a**, and **S9**). The calculated conductance of PP junctions also inversely correlates with the steric bulk of R (i.e., **Me** >> **^{t}Bu**, **Bn**, **C_7H_7**, **Tr**), as noted previously.[20,55] A closer inspection of each junction geometry (**Figure S10, Table S4**) reveals the Au-S bond of physisorbed contacts for all junctions except the

sterically unhindered **H** and **Me** is misaligned with, and so electronically decoupled from, the conjugated backbone π-orbitals. This decoupling can be seen in the transmission calculations, where the unoccupied resonances of **Me** are broadened relative to those for all other physisorbed junctions, which decreases transmission at E_F.

The low calculated conductance for **Tr** and **C_7H_7** (PP geometries) contrasts sharply with our experimental findings that the conductance of junctions formed from these compounds and **H** differ only by a factor of ~2. Importantly, this discrepancy supports our assertion that, under experimental conditions, the S-C(sp^3) bond in **Tr** and **C_7H_7** breaks resulting in the formation of chemisorbed contacts. Similarly, the low calculated conductance of **^{t}Bu** (PP) supports assignment of the high conductance peak in measurements of **^{t}Bu** to junctions of the CC type. In closing, we note that our model **Tr** junctions necessarily involve a frozen geometry (see **Figure S10**). When performing calculations using strict energy and force convergence criteria, all relaxed geometries for **Tr** show that the S-C(sp^3) bond spontaneously cleaves after attaching the gold clusters. This observation further highlights the propensity of this S-C(sp^3) bond to break in STM-BJ experiments.

In conclusion, we have identified that the most effective conditions to drive thioether S-C(sp^3) bond cleavage reactions at a gold surface involve non-polar solvents at elevated temperatures. While the role of the EEF appears convoluted with the attenuation of active sites for measurements in air, the apparent rate of this interfacial reaction can be significantly tuned by varying the stability of the carbocation leaving group. This work helps to further contextualize the possible role of carbocation leaving groups in the formation of Au-C(sp^2) linked molecular junctions from tetraphenylmethane-like compounds,[62] and gold-sulfur SAMs from -$SCPh_3$ functionalized precursors,[63] guiding future efforts in these areas as well as the study and exploitation of other Lewis-acid catalyzed reactions at metal surfaces. Our observation that the S-C(sp^3) bond in **Bn** does not readily cleave *in situ* supports the conclusions of previous studies in molecular electronics which have utilized similar motifs without knowledge of their reactive potential.

ASSOCIATED CONTENT

Electronic Supplementary Information (ESI) available: Additional experimental details, synthetic, conductance, and computational data, ^{1}H and ^{13}C{^{1}H} NMR spectra for all new compounds.

AUTHOR INFORMATION

Corresponding Authors

Daniel Hernangómez-Pérez – Email: d.hernangomez@nanogune.eu

María Camarasa-Gómez – Email: maria.camarasa@ehu.eus

Michael S. Inkpen – Email: inkpen@usc.edu

Notes

The authors declare no competing financial interest.

ACKNOWLEDGEMENTS

This work was primarily supported by funding from the University of Southern California (USC). D. H.-P. is grateful for funding from the Diputación Foral de Gipuzkoa through Grants 2023-FELL-000002-01, 2024-FELL-000009-01. M.C.-G. acknowledges support from the Diputación Foral de Gipuzkoa through Grant 2024-FELL-000007-01 and from the Gobierno Vasco-UPV/EHU Project No. IT1569-22. Instrumentation in the USC Chemistry Instrument Facility was acquired with support from the USC Research and Innovation Instrumentation Award Program. Additionally, funds provided by the NSF (DBI-0821671, CHE-0840366) and National Institute of Health (S10 RR25432) supported the acquisition of the NMR spectrometers used in our work.

REFERENCES

(1) Vogt, C.; Weckhuysen, B. M. The Concept of Active Site in Heterogeneous Catalysis. *Nat Rev Chem* **2022**, *6* (2), 89–111. https://doi.org/10.1038/s41570-021-00340-y.

(2) Friend, C. M.; Xu, B. Heterogeneous Catalysis: A Central Science for a Sustainable Future. *Acc. Chem. Res.* **2017**, *50* (3), 517–521. https://doi.org/10.1021/acs.accounts.6b00510.

(3) Chidsey, C. E. D. Free Energy and Temperature Dependence of Electron Transfer at the Metal-Electrolyte Interface. *Science* **1991**, *251* (4996), 919–922.

(4) Bain, C. D.; Whitesides, G. M. Molecular-Level Control over Surface Order in Self-Assembled Monolayer Films of Thiols on Gold. *Science* **1988**, *240* (4848), 62–63.

(5) Sullivan, T. P.; Huck, W. T. S. Reactions on Monolayers: Organic Synthesis in Two Dimensions. *European Journal of Organic Chemistry* **2003**, *2003* (1), 17–29. https://doi.org/10.1002/1099-0690(200301)2003:1<17::AID-EJOC17>3.0.CO;2-H.

(6) Wink, T.; Van Zuilen, S. J.; Bult, A.; Van Bennekom, W. P. Self-Assembled Monolayers for Biosensors. *Analyst* **1997**, *122* (4), 43–50. https://doi.org/10.1039/a606964i.

(7) Bullock, R. M.; Das, A. K.; Appel, A. M. Surface Immobilization of Molecular Electrocatalysts for Energy Conversion. *Chemistry - A European Journal* **2017**, *23* (32), 7626–7641. https://doi.org/10.1002/chem.201605066.

(8) Love, J. C.; Estroff, L. A.; Kriebel, J. K.; Nuzzo, R. G.; Whitesides, G. M. Self-Assembled Monolayers of Thiolates on Metals as a Form of Nanotechnology. *Chemical Reviews* **2005**, *105* (4), 1103–1170. https://doi.org/10.1021/cr0300789.

(9) Xu, B.; Tao, N. J. Measurement of Single-Molecule Resistance by Repeated Formation of Molecular Junctions. *Science* **2003**, *301* (5637), 1221–1223.

(10) Inkpen, M. S.; Liu, Z.; Li, H.; Campos, L. M.; Neaton, J. B.; Venkataraman, L. Non-Chemisorbed Gold–Sulfur Binding Prevails in Self-Assembled Monolayers. *Nature Chemistry* **2019**, *11*, 351–358.
(11) Cheng, Z. L.; Skouta, R.; Vazquez, H.; Widawsky, J. R.; Schneebeli, S.; Chen, W.; Hybertsen, M. S.; Breslow, R.; Venkataraman, L. In Situ Formation of Highly Conducting Covalent Au-C Contacts for Single-Molecule Junctions. *Nat. Nanotechnol.* **2011**, *6* (6), 353–357. http://www.nature.com/nnano/journal/v6/n6/abs/nnano.2011.66.html#supplementary-information.
(12) Millar, D.; Venkataraman, L.; Doerrer, L. H. Efficacy of Au−Au Contacts for Scanning Tunneling Microscopy Molecular Conductance Measurements. *J. Phys. Chem. C* **2007**, *111* (47), 17635–17639. https://doi.org/10.1021/jp0756101.
(13) Li, S.; Yu, H.; Chen, X.; Gewirth, A. A.; Moore, J. S.; Schroeder, C. M. Covalent Ag-C Bonding Contacts from Unprotected Terminal Acetylenes for Molecular Junctions. *Nano Letters* **2020**, *20* (7), 5490–5495. https://doi.org/10.1021/acs.nanolett.0c02015.
(14) Zang, Y.; Pinkard, A.; Liu, Z.-F.; Neaton, J. B.; Steigerwald, M. L.; Roy, X.; Venkataraman, L. Electronically Transparent Au–N Bonds for Molecular Junctions. *Journal of the American Chemical Society* **2017**, *139* (42), 14845–14848. https://doi.org/10.1021/jacs.7b08370.
(15) Ahn, S.; Aradhya, S. V.; Klausen, R. S.; Capozzi, B.; Roy, X.; Steigerwald, M. L.; Nuckolls, C.; Venkataraman, L. Electronic Transport and Mechanical Stability of Carboxyl Linked Single-Molecule Junctions. *Physical Chemistry Chemical Physics* **2012**, *14* (40), 13841. https://doi.org/10.1039/c2cp41578j.
(16) Starr, R. L.; Fu, T.; Doud, E. A.; Stone, I.; Roy, X.; Venkataraman, L. Gold–Carbon Contacts from Oxidative Addition of Aryl Iodides. *Journal of the American Chemical Society* **2020**, *142* (15), 7128–7133. https://doi.org/10.1021/jacs.0c01466.
(17) Czyszczon-Burton, T. M.; Montes, E.; Prana, J.; Lazar, S.; Rotthowe, N.; Chen, S. F.; Vázquez, H.; Inkpen, M. S. α,ω-Alkanedibromides Form Low Conductance Chemisorbed Junctions with Silver Electrodes. *J. Am. Chem. Soc.* **2024**, *146* (41), 28516–28526. https://doi.org/10.1021/jacs.4c11241.
(18) Stone, I. B.; Starr, R. L.; Hoffmann, N.; Wang, X.; Evans, A. M.; Nuckolls, C.; Lambert, T. H.; Steigerwald, M. L.; Berkelbach, T. C.; Roy, X.; Venkataraman, L. Interfacial Electric Fields Catalyze Ullmann Coupling Reactions on Gold Surfaces. *Chemical Science* **2022**, 20–24. https://doi.org/10.1039/d2sc03780g.
(19) Kim, L.; Czyszczon-Burton, T. M.; Nguyen, K. M.; Stukey, S.; Lazar, S.; Prana, J.; Miao, Z.; Park, S.; Chen, S. F.; Inkpen, M. S. Low Vapor Pressure Solvents for Single-Molecule Junction Measurements. *Nano Lett.* **2024**, *24* (32), 9998–10005. https://doi.org/10.1021/acs.nanolett.4c02786.
(20) Prana, J.; Kim, L.; Czyszczon-Burton, T.; Homann, G.; Chen, S.; Miao, Z.; Camarasa-Gomez, M.; Inkpen, M. Lewis-Acid Mediated Reactivity in Single-Molecule Junctions. *J. Am. Chem. Soc.* **2024**, *146* (48), 33265–33275. https://doi.org/10.1021/jacs.4c14176.
(21) Ghasemi, S.; Ornago, L.; Liasi, Z.; Johansen, M. B.; Von Buchwald, T. J.; Hillers-Bendtsen, A. E.; Van Der Poel, S.; Hölzel, H.; Wang, Z.; Amombo Noa, F. M.; Öhrström, L.; Mikkelsen, K. V.; Van Der Zant, H. S. J.; Lara-Avila, S.; Moth-Poulsen, K. Exploring the Impact of Select Anchor Groups for Norbornadiene/Quadricyclane Single-Molecule Switches. *J. Mater. Chem. C* **2023**, *11* (44), 15412–15418. https://doi.org/10.1039/D3TC02652C.
(22) Rashid, U.; Bro-Jørgensen, W.; Harilal, K.; Sreelakshmi, P.; Mondal, R. R.; Chittari Pisharam, V.; Parida, K. N.; Geetharani, K.; Hamill, J. M.; Kaliginedi, V. Chemistry of the Au–Thiol Interface through the Lens of Single-Molecule Flicker Noise

Measurements. *J. Am. Chem. Soc.* **2024**, *146* (13), 9063–9073. https://doi.org/10.1021/jacs.3c14079.
(23) Abboud, J.-L. M.; Alkorta, I.; Dávalos, J. Z.; Müller, P.; Quintanilla, E. Thermodynamic Stabilities of Carbocations. In *Advances in Physical Organic Chemistry*; Elsevier, 2002; Vol. 37, pp 57–135. https://doi.org/10.1016/S0065-3160(02)37002-3.
(24) Stuhr-Hansen, N. The Tert -Butyl Moiety—A Base Resistent Thiol Protecting Group Smoothly Replaced by the Labile Acetyl Moiety. *Synthetic Communications* **2003**, *33* (4), 641–646.
(25) Pijper, T. C.; Robertus, J.; Browne, W. R.; Feringa, B. L. Mild Ti-Mediated Transformation of t-Butyl Thio-Ethers into Thio-Acetates. *Org. Biomol. Chem.* **2015**, *13* (1), 265–268. https://doi.org/10.1039/C4OB02120G.
(26) Venkataraman, L.; Klare, J. E.; Nuckolls, C.; Hybertsen, M. S.; Steigerwald, M. L. Dependence of Single-Molecule Junction Conductance on Molecular Conformation. *Nature* **2006**, *442* (7105), 904–907. http://www.nature.com/nature/journal/v442/n7105/suppinfo/nature05037_S1.html.
(27) Miao, Z.; Quainoo, T.; Czyszczon-Burton, T. M.; Rotthowe, N.; Parr, J. M.; Liu, Z.; Inkpen, M. S. Charge Transport across Dynamic Covalent Chemical Bridges. *Nano Lett.* **2022**, *22* (20), 8331–8338. https://doi.org/10.1021/acs.nanolett.2c03288.
(28) Venkataraman, L.; Klare, J. E.; Tam, I. W.; Nuckolls, C.; Hybertsen, M. S.; Steigerwald, M. L. Single-Molecule Circuits with Well-Defined Molecular Conductance. *Nano Lett.* **2006**, *6* (3), 458–462. https://doi.org/10.1021/nl052373+.
(29) Fatemi, V.; Kamenetska, M.; Neaton, J. B.; Venkataraman, L. Environmental Control of Single-Molecule Junction Transport. *Nano Letters* **2011**, *11* (5), 1988–1992. https://doi.org/10.1021/nl200324e.
(30) He, J.; Sankey, O.; Lee, M.; Tao, N.; Li, X.; Lindsay, S. Measuring Single Molecule Conductance with Break Junctions. *Faraday Discuss.* **2006**, *131* (0), 145–154. https://doi.org/10.1039/b508434m.
(31) Sedrez, P. C.; Noriega Sanchez, C. J.; Da Silva, M. J.; Barbosa, J. R. Addendum to "Dielectric Constant of Mixtures of Carbon Dioxide and n-Dodecane Between 283 K and 343 K, Int. J. Thermophysics 41, 26, 2020": Complementary Results for Mixtures of Carbon Dioxide and Squalane Between 283 K and 343 K. *Int J Thermophys* **2020**, *41* (6), 69. https://doi.org/10.1007/s10765-020-02640-9.
(32) Haynes, W. M. *CRC Handbook of Chemistry and Physics*; CRC Press, 2014.
(33) Clayden, J.; Greeves, N.; Warren, S. *Organic Chemistry*; Oxford University Press, 2012.
(34) Smoluchowski, R. Anisotropy of the Electronic Work Function of Metals. *Physical Review* **1941**, *60* (9), 661–674. https://doi.org/10.1103/PhysRev.60.661.
(35) Sykes, E. C. H.; Mantooth, B. A.; Han, P.; Donhauser, Z. J.; Weiss, P. S. Substrate-Mediated Intermolecular Interactions: A Quantitative Single Molecule Analysis. *J. Am. Chem. Soc.* **2005**, *127* (19), 7255–7260. https://doi.org/10.1021/ja0472331.
(36) Costello, C. K.; Kung, M. C.; Oh, H.-S.; Wang, Y.; Kung, H. H. Nature of the Active Site for CO Oxidation on Highly Active Au/γ-Al2O3. *Applied Catalysis A: General* **2002**, *232*, 159–168.
(37) Schoenbaum, C. A.; Schwartz, D. K.; Medlin, J. W. Controlling the Surface Environment of Heterogeneous Catalysts Using Self-Assembled Monolayers. *Accounts of Chemical Research* **2014**, *47* (4), 1438–1445. https://doi.org/10.1021/ar500029y.
(38) Li, G.; Wang, B.; Resasco, D. E. Solvent Effects on Catalytic Reactions and Related Phenomena at Liquid-Solid Interfaces. *Surface Science Reports* **2021**, *76* (4), 100541. https://doi.org/10.1016/j.surfrep.2021.100541.

(39) Tsiper, E. V.; Soos, Z. G.; Gao, W.; Kahn, A. Eletronic Polarization at Surfaces and Thin Films of Organic Molecular Crystals: PTCDA. *Chemical Physics Letters* **2002**, *360* (1–2), 47–52. https://doi.org/10.1016/S0009-2614(02)00774-1.
(40) Sorenson, S. A.; Patrow, J. G.; Dawlaty, J. M. Solvation Reaction Field at the Interface Measured by Vibrational Sum Frequency Generation Spectroscopy. *Journal of the American Chemical Society* **2017**, *139* (6), 2369–2378. https://doi.org/10.1021/jacs.6b11940.
(41) Orchanian, N. M.; Guizzo, S.; Steigerwald, M. L.; Nuckolls, C.; Venkataraman, L. Electric-Field-Induced Coupling of Aryl Iodides with a Nickel(0) Complex. *Chemical Communications* **2022**, *58*, 12556–12559. https://doi.org/10.1039/d2cc03671a.
(42) Dutta Dubey, K.; Stuyver, T.; Kalita, S.; Shaik, S. Solvent Organization and Rate Regulation of a Menshutkin Reaction by Oriented External Electric Fields Are Revealed by Combined MD and QM/MM Calculations. *J. Am. Chem. Soc.* **2020**, *142* (22), 9955–9965. https://doi.org/10.1021/jacs.9b13029.
(43) Hollenstein, S.; Laube, T. Crystal Structure of the Tert-Butyl Cation. *J. Am. Chem. Soc.* **1993**, *115* (16), 7240–7245. https://doi.org/10.1021/ja00069a023.
(44) Aziz, M.; Prindle, C. R.; Lee, W.; Zhang, B.; Schaack, C.; Steigerwald, M. L.; Zandkarimi, F.; Nuckolls, C.; Venkataraman, L. Evaluating the Ability of External Electric Fields to Accelerate Reactions in Solution. *J. Phys. Chem. B* **2024**, acs.jpcb.4c04864. https://doi.org/10.1021/acs.jpcb.4c04864.
(45) Otomo, T.; Suzuki, H.; Iida, R.; Takayanagi, T. SN1 Reaction Mechanisms of Tert-Butyl Chloride in Aqueous Solution: What Can Be Learned from Reaction Path Search Calculations and Trajectory Calculations for Small Hydrated Clusters? *Computational and Theoretical Chemistry* **2021**, *1201*, 113278. https://doi.org/10.1016/j.comptc.2021.113278.
(46) Olah, G. A. Carbocations and Electrophilic Reactions. *Angew. Chem. Int. Ed. Engl.* **1973**, *12* (3), 173–212. https://doi.org/10.1002/anie.197301731.
(47) Lifshitz, C. Tropylium Ion Formation from Toluene: Solution of an Old Problem in Organic Mass Spectrometry. *Acc. Chem. Res.* **1994**, *27* (5), 138–144. https://doi.org/10.1021/ar00041a004.
(48) Sharma, D. K. S.; Kebarle, P. Stability and Reactivity of the Benzyl and Tropylium Cations in the Gas Phase. *Can. J. Chem.* **1981**, *59* (11), 1592–1601. https://doi.org/10.1139/v81-235.
(49) Leary, E.; Zotti, L. A.; Miguel, D.; Márquez, I. R.; Palomino-Ruiz, L.; Cuerva, J. M.; Rubio-Bollinger, G.; González, M. T.; Agrait, N. The Role of Oligomeric Gold–Thiolate Units in Single-Molecule Junctions of Thiol-Anchored Molecules. *The Journal of Physical Chemistry C* **2018**, *122* (6), 3211–3218. https://doi.org/10.1021/acs.jpcc.7b11104.
(50) He, J.; Chen, F.; Liddell, P. A.; Andréasson, J.; Straight, S. D.; Gust, D.; Moore, T. A.; Moore, A. L.; Li, J.; Sankey, O. F.; Lindsay, S. M. Switching of a Photochromic Molecule on Gold Electrodes: Single-Molecule Measurements. *Nanotechnology* **2005**, *16* (6), 695–702. https://doi.org/10.1088/0957-4484/16/6/012.
(51) Bowers, C. M.; Rappoport, D.; Baghbanzadeh, M.; Simeone, F. C.; Liao, K.-C.; Semenov, S. N.; Żaba, T.; Cyganik, P.; Aspuru-Guzik, A.; Whitesides, G. M. Tunneling across SAMs Containing Oligophenyl Groups. *J. Phys. Chem. C* **2016**, *120* (21), 11331–11337. https://doi.org/10.1021/acs.jpcc.6b01253.
(52) Nguyen, Q. V.; Xie, Z.; Daniel Frisbie, C. Quantifying Molecular Structure-Tunneling Conductance Relationships: Oligophenylene Dimethanethiol vs Oligophenylene Dithiol Molecular Junctions. *Journal of Physical Chemistry C* **2021**, *125* (7), 4292–4298. https://doi.org/10.1021/acs.jpcc.0c11514.

(53) Vazquez, H.; Skouta, R.; Schneebeli, S.; Kamenetska, M.; Breslow, R.; Venkataraman, L.; Hybertsen, M. S. Probing the Conductance Superposition Law in Single-Molecule Circuits with Parallel Paths. *Nat. Nanotechnol.* **2012**, *7* (10), 663–667. http://www.nature.com/nnano/journal/v7/n10/abs/nnano.2012.147.html#supplementary-information.
(54) Park, Y. S.; Widawsky, J. R.; Kamenetska, M.; Steigerwald, M. L.; Hybertsen, M. S.; Nuckolls, C.; Venkataraman, L. Frustrated Rotations in Single-Molecule Junctions. *J. Am. Chem. Soc.* **2009**, *131* (31), 10820–10821. https://doi.org/10.1021/ja903731m.
(55) Batra, A.; Darancet, P.; Chen, Q.; Meisner, J. S.; Widawsky, J. R.; Neaton, J. B.; Nuckolls, C.; Venkataraman, L. Tuning Rectification in Single-Molecular Diodes. *Nano Lett.* **2013**, *13* (12), 6233–6237. https://doi.org/10.1021/nl403698m.
(56) Blum, V.; Gehrke, R.; Hanke, F.; Havu, P.; Havu, V.; Ren, X.; Reuter, K.; Scheffler, M. Ab Initio Molecular Simulations with Numeric Atom-Centered Orbitals. *Computer Physics Communications* **2009**, *180* (11), 2175–2196. https://doi.org/10.1016/j.cpc.2009.06.022.
(57) Camarasa-Gómez, M.; Hernangómez-Pérez, D.; Evers, F. Spin–Orbit Torque in Single-Molecule Junctions from Ab Initio. *J. Phys. Chem. Lett.* **2024**, *15* (21), 5747–5753.
(58) Arnold, A.; Weigend, F.; Evers, F. Quantum Chemistry Calculations for Molecules Coupled to Reservoirs: Formalism, Implementation, and Application to Benzenedithiol. *The Journal of Chemical Physics* **2007**, *126* (17), 174101. https://doi.org/10.1063/1.2716664.
(59) Bagrets, A. Spin-Polarized Electron Transport Across Metal–Organic Molecules: A Density Functional Theory Approach. *Journal of Chemical Theory and Computation* **2013**, *9* (6), 2801–2815. https://doi.org/10.1021/ct4000263.
(60) Thoss, M.; Evers, F. Perspective: Theory of Quantum Transport in Molecular Junctions. *The Journal of Chemical Physics* **2018**, *148* (3), 30901. https://doi.org/10.1063/1.5003306.
(61) Evers, F.; Korytár, R.; Tewari, S.; Van Ruitenbeek, J. M. Advances and Challenges in Single-Molecule Electron Transport. *Reviews of Modern Physics* **2020**, *92* (3), 35001. https://doi.org/10.1103/RevModPhys.92.035001.
(62) Zagami, L.; Avedian, C.; Sharma, M.; Fraire, A.; Olivar, C.; Hernangómez-Pérez, D.; Inkpen, M. Isotropically Conducting Tetraaryl Osmium(IV), Silane, and Methane Molecular Wire Junctions. ChemRxiv February 10, 2025. https://doi.org/10.26434/chemrxiv-2025-cjj3v.
(63) Inman, C. E.; Reed, S. M.; Hutchison, J. E. In Situ Deprotection and Assembly of S-Tritylalkanethiols on Gold Yields Monolayers Comparable to Those Prepared Directly from Alkanethiols. *Langmuir* **2004**, *20* (21), 9144–9150. https://doi.org/10.1021/la049627b.